FOI-R--1500--SE
December 2004
ISSN 1650-1942
Technical report

L. Sjöqvist, E. Hällstig, U. Larsson, L. Allard

Activities in adaptive optics – Characterisation of components

Sensor Technology
SE-581 11 Linköping

SWEDISH DEFENCE RESEARCH AGENCY

Sensor Technology
P.O. Box 1165
SE-581 11 Linköping

FOI-R--1500--SE

December 2004

ISSN 1650-1942

Technical report

L. Sjöqvist, E. Hällstig, U. Larsson, L. Allard

Activities in adaptive optics – Characterisation of components

Issuing organization
FOI – Swedish Defence Research Agency
Sensor Technology
P.O. Box 1165
SE-581 11 Linköping

Report number, ISRN
FOI-R--1500--SE

Report type
Technical report

Research area code
61 Electronic Warfare including Electromagnetic Weapons and Protection

Month year
December 2004

Project no.
E3020

Sub area code
61 Electronic Warfare including Electromagnetic Weapons and Protection

Sub area code 2

Author/s (editor/s)
L. Sjöqvist
E. Hällstig
U. Larsson
L. Allard

Project manager
Ove Steinvall

Approved by
Lena Klasén

Sponsoring agency
HKV

Scientifically and technically responsible
Lars Sjöqvist

Report title
Activities in adaptive optics – Characterisation of components

Abstract (not more than 200 words)

Adaptive optics (AO) techniques have evolved rapidly during recent years due to development of new components. In laser countermeasures perturbations due to atmospheric turbulence, engine plumes and aero-optical effects may degrade system performance dramatically. Adaptive optics methods provide schemes to compensate for perturbations and improve system performance. This could be an alternative to scaling of the laser power which can be difficult to achieve from a technical point of view.

In order to evaluate adaptive optics in laser countermeasure applications components and their performance need to be characterised from an experimental point of view. Proper modelling is also required to facilitate the understanding of the benefits of implementing adaptive optics schemes. The components include the wavefront sensor and the correcting element. The Shack-Hartmann wavefront sensor and a deformable membrane mirror were considered in this report. In addition, a piezo-electric tip-tilt mirror was briefly studied. The report covers activitities focusing on characterisation of the components. A setup for a cosed-loop laboratory AO system is briefly discussed.

Keywords
Adaptive optics, deformable mirror, Shack-Hartmann, wavefront sensor

Further bibliographic information

Language English

ISSN 1650-1942

Pages 33 p.

Price acc. to pricelist

Utgivare	Rapportnummer, ISRN	Klassificering
Totalförsvarets Forskningsinstitut - FOI	FOI-R--1500--SE	Teknisk rapport
Sensorteknik	**Forskningsområde**	
Box 1165	6. Telekrig och vilseledning	
581 11 Linköping	**Månad, år**	**Projektnummer**
	December 2004	E3020
	Delområde	
	61 Telekrigföring med EM-vapen och skydd	
	Delområde 2	

Författare/redaktör	Projektledare
L. Sjöqvist	Ove Steinvall
E. Hällstig	**Godkänd av**
U. Larsson	Lena Klasén
L. Allard	**Uppdragsgivare/kundbeteckning**
	HKV
	Tekniskt och/eller vetenskapligt ansvarig
	Lars Sjöqvist

Rapportens titel (i översättning)

Adaptiv optik – Karakterisering av komponenter

Sammanfattning (högst 200 ord)

Adaptiv optikområdet (AO) har utvecklats snabbt under de senaste åren pga utvecklandet av nya komponenter. Vid användning av laserbaserade motmedel existerar störningar från turbulens i atmosfären, motorplymer och aero-optiska effekter vilka kan försämra systemprestanda väsentligt. Metoder baserade på adaptiv optik kan erbjuda nya möjligheter att kompensera dessa störningar och förbättra prestanda. Tekniken kan vara ett alternativ till att skala upp lasereffekten något som kan vara tekniskt svårt i vissa våglängdsområden.

För att kunna utvärdera AO-tekniken i laserbaserade motmedelstillämpningar behöver komponenters prestanda karakteriseras experimentellt. Utveckling av modeller är också nödvändigt för att underlätta analysen för att förstå fördelar som kan uppnås med att implementera AO-teknik. Komponenter inkluderar här vågfrontssensorer och korrigerande element. En Shack-Hartmann vågfrontssensor, en deformerbar spegel samt en tip-tiltspegel har studerats i den här rapporten. Rapporten sammanfattar resultat av karakterisering av komponenterna. En AO-uppställning för att demonstrera sluten loop i labbet diskuteras översiktligt.

Nyckelord

Adaptiv optik, deformerbar spegel, Shack-Hartmann, vågfrontsensor

Övriga bibliografiska uppgifter	Språk Engelska
ISSN 1650-1942	**Antal sidor:** 33 s.
Distribution enligt missiv	**Pris: Enligt prislista**

CONTENT

1 INTRODUCTION

Laser countermeasures can be used to protect airborne platforms from missile threats. Considering platforms, such as large transport aircrafts, helicopters and fast jets, directed infrared laser countermeasure (DIRCM) systems are under development. One important issue related to the performance of DIRCM systems is the influence from external and platform induced perturbations. Several perturbations exist which may degrade the performance of a laser countermeasure system. Atmospheric turbulence effects, caused by variation of the index of refraction in air, cause beam broadening and beam wandering phenomena. Depending on the turbulence strength the laser beam quality is affected and the brightness on the target can be considerably reduced. Other perturbations related to platform characteristics include e.g. aero-optical effects and strong turbulence associated with movement of hot air masses in close vicinity of a jet engine plume considering airborne platforms. Perturbations also occur in optical components and within the laser source. The major perturbation attributed to airborne platforms is due to mechanical vibration causing line of sight beam jitter. The acquisition, pointing and tracking (APT) head is a critical part of the laser countermeasure system. The APT simultaneously track and direct the beam onto an approaching target. The traditional APT consists of a line of sight (LOS) beam director using a gimballed configuration. *Adaptive Optics (AO)* techniques are presently studied for implementation in APT technology for laser counter measures and similar applications utilising a laser transmitter (Figure 1).

During recent years adaptive optics has been explored in different applications ranging from free-space optical communications to medical applications. The adaptive optics techniques have by tradition been used in the astronomical community and in laser weapon research. Rapid development of new components has made the technique viable for other applications. New components and principles of AO have been studied extensively in the laboratory and in technical demonstrations during the recent years. One example of a major effort including AO is the Airborne Laser Program (ABL) program. Another example is a recent CEPA8 project within the WEAG constellation aiming to study the effect of using AO in a directed infrared countermeasure (DIRCM) APT[1]. The impetus for including AO principles and components in an APT is the urge to increase the brightness on the target and, hence, in a laser countermeasure application to increase the signal to jammer ratio. Another application is related to active beam shaping in laser transmitters. The use of AO techniques in DIRCM applications have been discussed previously[2].

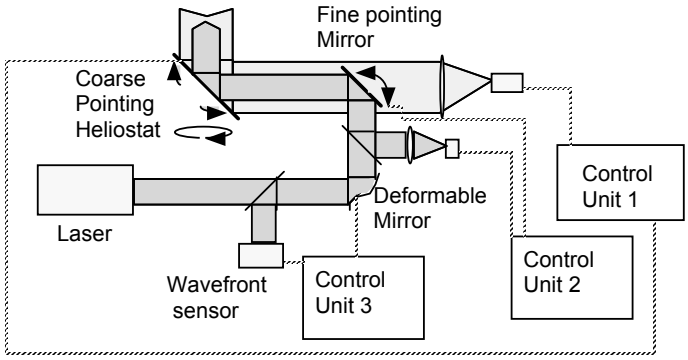

Figure 1 Schematic adaptive optics system showing the different sub-components. From ref. [1]

The adaptive optic system consist of three major parts; a wavefront sensing device called the wavefront sensor (WFS), wavefront correcting elements and the control algorithm and control system. The wavefront sensing aims to determine the deviations from an un-perturbed

wavefront in order to apply a necessary compensation scheme. Several wavefront sensing techniques exist (based on e.g. sensing the slope or the curvature of the wavefront) and have been discussed in the literature[3]. The Shack-Hartmann (SH) sensor is commonly utilised for sensing the local slope of the wavefront[4].The SH WFS uses an array of micro lenses to estimate the deviations of the wavefront. By combining the lens array with a CCD detector the wavefront perturbations can be determined.

The wavefront can be corrected by a deformable, or segmented, mirror capable of generating a correction which corresponds to the complex conjugate of the perturbed wavefront[5]. Deformable mirrors (DM) have attracted considerable interest recently and are commonly employed for this purpose. The deformable mirror can be manufactured as a monolithic device or as a membrane mirror. The monolithic DM can e.g. be a biomorphic mirror driven by piezoelectric actuators having the advantage of high robustness although possesses a relatively high price. Recently, membrane mirrors with a thin metallic membrane situated over an array of electro-static actuators have been manufactured. These simple DM can be used in laboratory AO setups to investigate performance and evaluate AO schemes in different applications. The drawback using DM membrane mirrors is their sensitivity to environmental effects preventing them to be used in real applications whereas harsh environments are present. The lowest order correction is defined by the tip-tilt error frequently corrected by a separate tip-tilt mirror. The WFS and the correcting elements need to be controlled in a precise manner and a suitable reconstruction scheme is required. The first step in implementing AO techniques in an application includes the setup of a laboratory system on an optical table aiming to evaluate schemes and principles. Before the components can be incorporated in a closed-loop setup each component needs to be studied and evaluated experimentally in order to predict the performance of the AO system.

In this report activities aiming to understand the performance of components constituting an AO system is described. Components including a Shack-Hartmann WFS, a micromachined membrane deformable mirror (DM) and a tip-tilt mirror have been studied experimentally. The emphasis has been on the DM mirror. In addition, schemes for reconstruction and control have been evaluated. Modelling activities involving different components are described. A scheme for assembling a laboratory closed-loop AO-system is proposed. The long-term effort motivating the presented study is to evaluate AO-principles in laser countermeasure applications.

2 COMPONENTS

The basic components used in an AO system are the WFS and the correcting element (or elements if several are used). The performance of the individual components needs to be carefully evaluated in order to design a proper AO system. In this study the correctable elements investigated were a piezoelectric tip-tilt mirror and membrane deformable mirror. The WFS was a conventional Shack-Hartman sensor.

2.1 Tip-tilt mirror

Two techniques frequently used for tip-tilt mirrors are based on voice coil actuators or piezoelectric materials. The voice coil mirror has some advantages providing a larger deflection angle. The piezoelectric mirror, on the other hand, is fabricated using mature technology since piezoelectric components have been extensively utilised in positioning applications during a long period of time. The tip-tilt mirror described and studied in this work is a piezoelectric tip-tilt mirror with large deflection range.

The tip-tilt mirror was a two-axis piezoelectric mirror model S-334.2SL fabricated by Physike Instrument, GmbH. The mirror had a clear aperture diameter of 10 mm coated with Al (Figure 2A). The mirror consist of a 2 mm thick BK7 glass having a surface error less that λ/5 and a reflectivity larger than 98% @ 500 to 2000 nm. The mirror could be operated in open- or closed loop conditions. In the closed-loop mode internal strain gauge sensors are utilised. In the final optical setup of the AO system the feedback to the tip-tilt mirror will be provided by a positional sensitive detector such as a quadrant detector (quad) or a positional sensitive device (PSD). The open loop resonance frequency of the mirror was specified to 1 kHz. However, according to the manufacturer the mirror can only be driven to about one third of the resonance frequency depending on the mechanical load. The specified accuracy (open-loop) is better than 0.5 μrad and the maximal deflection range is ±25 mrad.

The mirror drive signals were provided using a PI PZ48E three channel amplifier. The feedback sensors in the mirror were disconnected in the setup i.e. corresponding to running the mirror in open-loop mode. One mirror channel was set to +100 V, whereas the two other channels were driven by input voltages in the range, 0 to 100 V. The amplifier supplied a bias to be set to all of the channels. A software application was written in Labview designed to feed the mirror with different drive signals. A laptop computer with a D/A- card was attached to the amplifier to generate the drive voltages. The dedicated software facilitates generation of more complicated scan pattern. In addition to using software control a function generator was employed to generate drive signals.

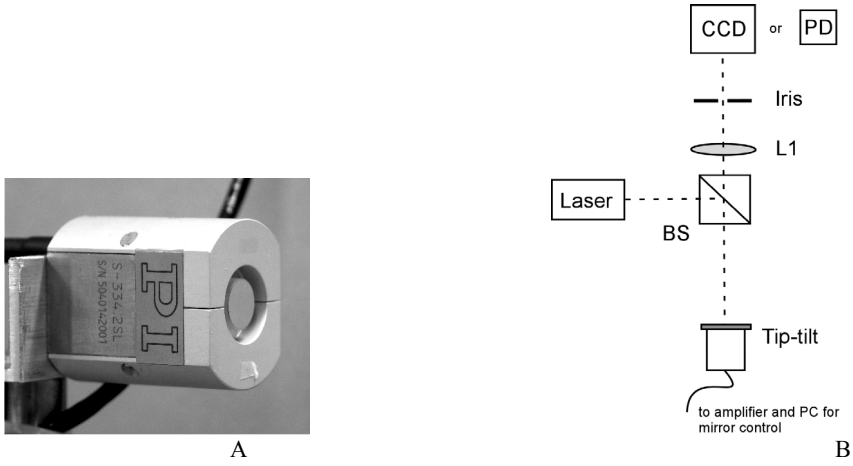

Figure 2 A) Photograph showing the tip-tilt mirror. B) Experimental setup used to study tip-tilt mirror performance.

The experimental setup used to study tip-tilt mirror performance is shown in Figure 2B. The temporal properties were investigated using a photo detector. The photo detector was replaced by a CCD camera when spatial properties were studied. Important mirror performance parameters include the deflection range, the resolution and the temporal bandwidth.

The temporal properties of the tip-tilt mirror were tested up to 350 Hz using the setup above. An example illustrating the behaviour of the mirror is shown in Figure 3A whereas a sinusoidal drive voltage is applied at 300 Hz and a mirror deflection of ±2.5 mrad. Note that the optical signal exhibits two peaks for each period since the beam passes the iris twice for each period of the drive signal. Another example of the properties of the tip-tilt mirror showing the beam deflection versus the applied voltage (single-channel) is depicted in Figure 3B. The beam motion was registered by keeping one channel at constant voltage and varying the voltage on the second channel. The calculated position of the beam centroid can be fitted to a linear function i.e. the tip-tilt mirror shows a linear response with respect to the deflection angle. The linear response was observed within the full working range of the mirror.

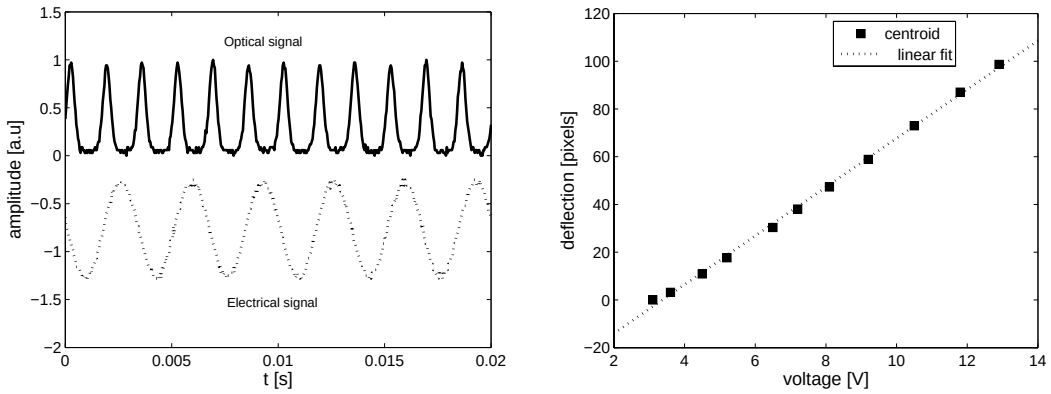

Figure 3 A) Temporal properties of the tip-tilt mirror. The upper trace shows the optical signal and the lower the electrical drive signal at 300 Hz using a sinusoidal drive voltage. B) Beam displacement registered by a CCD camera as function of the applied voltage (single-channel).

2.2 Deformable mirror

The results presented in this paragraph were initially described in a previous preliminary study and is presented in detail in a work soon to be available[6,7]. We review some of the results from the latter study more in detail describing mirror characterisation, wavefront reconstruction and Zernike polynomial generation.

Micromachined deformable membrane (DM) mirrors are low-cost adaptive optics correction components. The technology for fabrication of these types of devices is residing on the experience gained from silicon processing technology, which has developed rapidly during the recent years. The micromachined membrane mirror consists of two parts; a thin deformable membrane placed onto an actuator structure usually mounted on a PCB board or silicon wafer, which provides a simple technical solution[5]. The two parts are separated by an air gap using spacers. An example of a commercial micromachined membrane mirror is shown in Figure 4. Applying a voltage of the order 0-215 V to the actuator electrodes the deflection of the membrane can be controlled. Both single actuator and multi-channel devices have been developed. A frequency response up to 1 kHz is common and the deflection range is 10 to 20 μm. The limited numbers of actuators (approximately 37 to 120) make these components most suitable for low order wavefront corrections. Moreover, the relatively high drive voltage makes separate control electronics boards unavoidable.

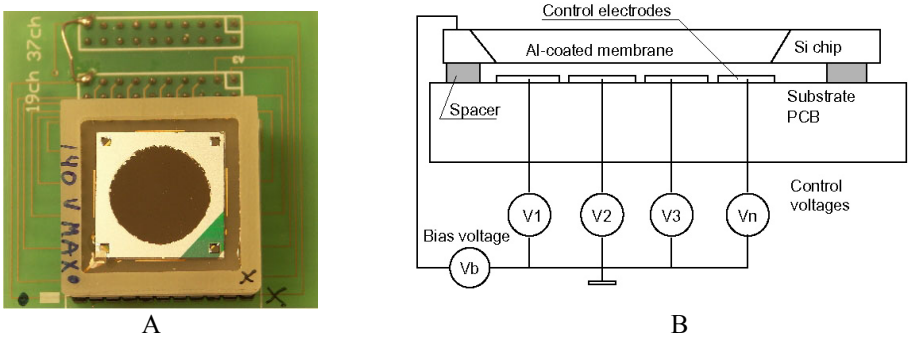

Figure 4 a) Photograph showing a 37 channel membrane DM from OKO Technologies. b) Schematic layout of the micromachined DM mirror.

The deformable mirror investigated in the study was manufactured by OKO Technologies[1], and consisted of 37 separate channels. The mirror was a silicon nitride membrane mounted upon a PCB substrate. An aluminium coating is placed on the top of the mirror membrane. The mirror has a circular aperture of approximately 15 mm in diameter. A dedicated program written in C^{++} controlled the mirror. A graphical interface was created whereas the voltage to each individual electrode could be controlled. An amplifier board developed by OKO Technologies Inc. drove the mirror. The output voltages to the amplifiers were controlled via a digital-to-analogue converter (PCI board) attached to a PC. The graphical interface provided a direct access to the output port on the PCI board.

2.2.1 Interferometer measurements

The wavefront characteristics can be analysed by studying fringes in an interferometer setup. Among the simplest interferometers is the Twyman-Green configuration shown in Figure 5. A HeNe laser is used as a light source in this setup. The optical path length (OPL) in the interferometer can be altered by physically moving the DM or the reference mirror. A tilt term can also be introduced by the reference mirror. A spatial filter using a microscope objective and a pinhole cleans the wavefront of the light used for analysis. Two positive lenses were used to collimate the beam before it entered the interferometer arms separated by a non-polarising beam splitter. A CCD camera captured the interferograms and an additional PC was connected to the set-up to capture interferograms. The mirror was attached to a high voltage amplifier and a PC for providing appropriate drive signals.

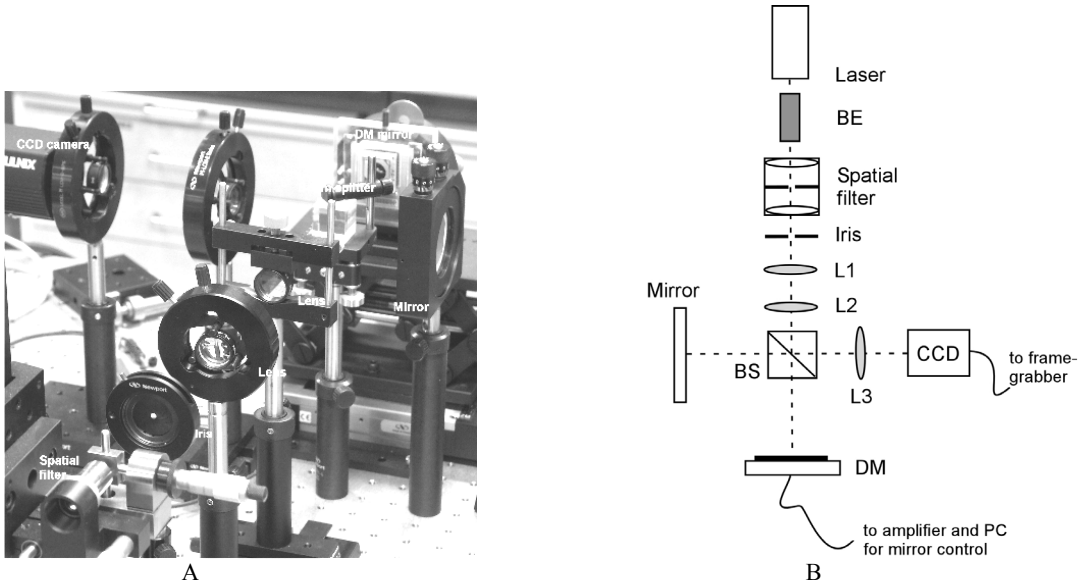

Figure 5 A) Photograph showing the deformable mirror in the interferometer setup. B) Interferometer setup for characterisation of the membrane DM. The following abbreviations are used: BS-beam splitter, L1, L2 and L3–lenses and BE–beam expander. A HeNe laser (λ = 633 nm) was used in the setup.

2.2.2 Fringe analysis using Fourier decomposition

The deflection of the deformable mirror was initially analysed using the commercial software named QuickFringe[8]. This program facilitates fringe analysis and can be utilised importing experimental interferometer data. The program automatically removes piston and tip/tilt terms and determines the decomposition of the wavefront in terms of Zernike polynomials. The output data after analysis is a set comprising the Zernike polynomials and weighting coefficients

[1] http://www.okotech.com/

representing the wavefront. The QuickFringe program was only used initially in the analysis of the deflection of the deformable mirror since the program could not be implemented with dedicated software for simultaneous mirror control and analysis. However, the results from QuickFringe were compared with the Fourier transform method described below and the agreement between the two methods was found to be satisfactorily. An example comparing data between the approaches is shown in Figure 6.

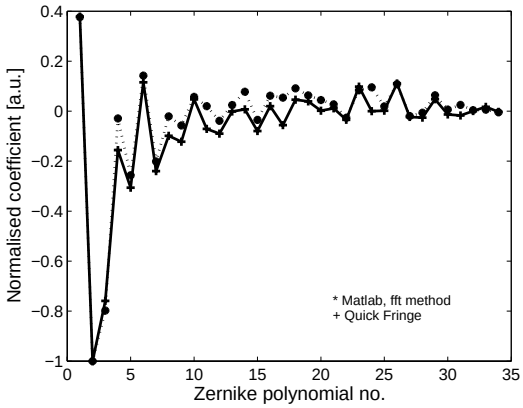

Figure 6 Comparison between interferogram analysed by the QuickFringe program and the Matlab developed software (see below). The interferograms were generated by the deformable mirror.

The fringe pattern observed using an interferometer setup can be analysed using a Fourier decomposition method. The interferogram can be expressed mathematically by adding the field from the reference beam, U_1, to a probe beam, U_2. Using a scalar field notation this can be expressed as

$$I = |U_1 + U_2|^2 = |U_1|^2 + |U_2|^2 + U_1 \cdot U_2^* + U_1^* \cdot U_2 \qquad (1)$$

where U_i represent the complex field amplitude of the reference and probe beam, respectively. The first two terms in (1) represent the intensity of the reference and the probe whereas the third and fourth terms give rise to the interference pattern observed on the CCD. In the reconstruction scheme the reference beam illuminates the recorded intensity

$$U_1 \cdot I = U_1 \cdot I_1 + U_1 \cdot I_2 + U_1^2 \cdot U_2^* + I_1 \cdot U_2 . \qquad (2)$$

which can be expressed as

$$U_1 \cdot I = U_1 \cdot (I_1 + I_2) + I_1 \cdot (U_2^* + U_2) \qquad (3)$$

using the fact that $I_1 = U_1 \cdot U_1$ for an ideal reference beam (i.e. no aberrations). If eq. (3) is Fourier transformed the far-field distribution can be written as

$$\hat{U}_1 \otimes \hat{I} = \hat{U}_1 \otimes (\hat{I}_1 + \hat{I}_2) + \hat{I}_1 \otimes \hat{U}_2^* + \hat{I}_1 \otimes \hat{U}_2 \qquad (4)$$

where the ^ and ⊗ denote the Fourier transform and convolution operation. The three terms in eq. (4) represent 0, -1 and +1 diffraction order, respectively. Assuming a uniform beam reference (i.e. the Fourier transform is represented by delta function) the following expression can be filtered out:

$$\hat{I} = (\hat{I}_1 + \hat{I}_2) + \hat{U}_2^* + \hat{U}_2 . \quad (5)$$

The fields, U_2 or U_2^*, can now be determined by locating a selecting aperture over the chosen diffraction order in the Fourier plane. This method requires that the ± 1 orders are separable from the 0 order i.e. no overlap. This can be accomplished by tilting the reference beam.

An example showing two simulated interferograms is depicted in Figure 7. The typical interferometer pattern observed for spherical aberrations is exemplified in Figure 7A. In this case an ideal reference beam was used and the distorted beam exhibited 3 waves of spherical aberrations. A slight distortion of this pattern can be observed when a residual tilt aberration is present in the reference beam (Figure 7B).

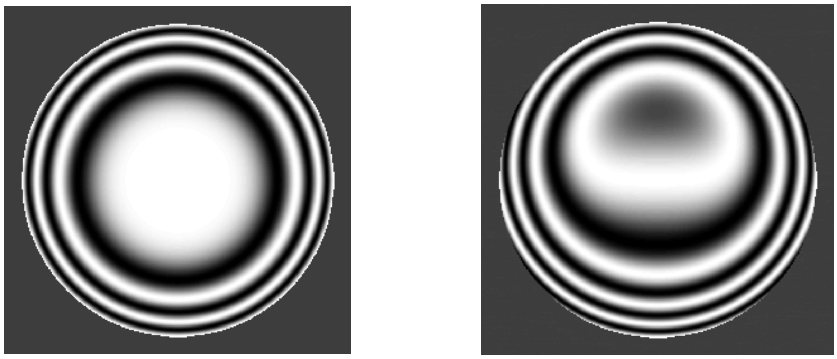

A B

Figure 7 A) Simulated interferogram using an ideal probe beam and aberrated beam with spherical distortion of 3 waves (at λ = 633 nm). B) Same parameters as in a) but 1 wave of tilt aberrations added.

The method described above for reconstruction of recorded interferograms has been tested on simulated aberrations. An example showing a reconstruction using the Fourier decomposition method is depicted in Figure 8. The introduced tilt effectively separates the ±1 orders from the central order. The reconstructed interferogram closely resembles the original in this simple example. The linear tilt can be removed from the interferogram showing only the spherical aberration (Figure 8C). This method was used in characterisations of the DM mirror.

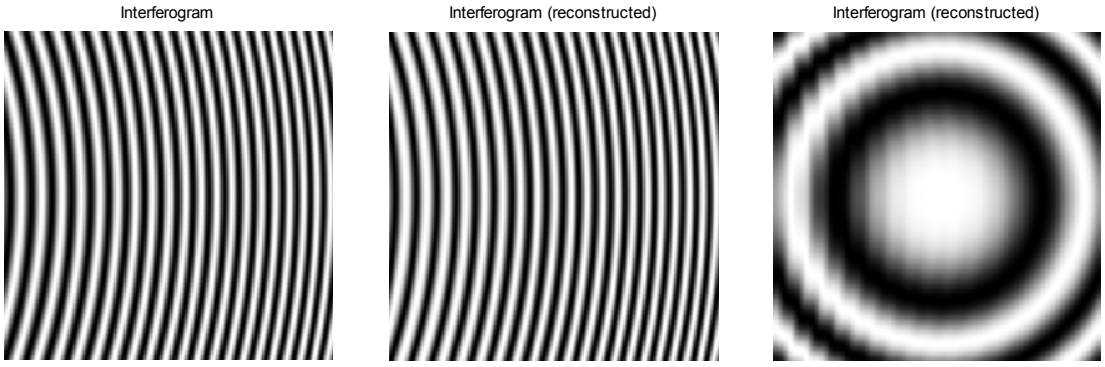

A B C

Figure 8 A) Simulated interference pattern assuming the following parameters: λ = 1000 nm, a spherical aberration corresponding to e lens with focal length 10 m, 10x10 mm^2 field dimension and 2 mrad tilt. B) Reconstructed interferogram using the method described above. C) Same as in B) but with the tilt term removed.

The method is exemplified in the experimental section below showing an interferogram generated in the deformable mirror setup.

2.2.3 Mirror wavefront reconstruction scheme

In order to control the mirror a scheme for wavefront reconstruction needs to be designed and verified[9,10,11]. The main purpose with the wavefront reconstruction scheme is to find methods which interpret a certain voltage distribution applied to the actuators into a given deflection of the mirror membrane expressible in e.g. Zernike polynomials.

If the mirror aperture is circular (as in the case of the deformable mirror) it is appropriate to use a Zernike polynomial expansion expressing the mirror surface by the linear expansion

$$\Phi(x,y)=\sum_{k=1}^{\infty}a_k z_k(x,y) \tag{6}$$

where a_k are the Zernike coefficients and z_k the Zernike polynomials as basis functions. An example showing some representative Zernike polynomials is depicted in Figure 9. Usually a limited number of Zernike polynomials are used to represent the mirror implying that eq. (6) can be written as

$$\Phi(x,y)=\sum_{k=1}^{N_M}a_k z_k(x,y)+\varepsilon \tag{7}$$

where N_M is the number of utilised Zernike polynomials and ε is an error term due to the fact that only a limited Zernike basis is used in the expansion above. Assuming that the mirror can be rather accurately described by the N_M first Zernike polynomials the error term ε can be neglected. Suppose now that the mirror deflection can be described by a set of influence functions, $\varphi_l(x,y)$, which can be used to define the mirror surface under action of the control signals c_l according to

$$\Phi(x,y)=\sum_{l=1}^{N_P}\varphi_l(x,y)\cdot c_l \tag{8}$$

where N_P is the number of actuators. The response, or influence functions, can be expanded in Zernike polynomials according to

$$\varphi_l(x,y)=\sum_{k=1}^{N_M}r_{kl}z_k(x,y) \tag{9}$$

where r_{kl} is a set of expansion coefficients describing the acting of the influence functions on the mirror. By combining eqs. (8) and (9) the following relation is obtained

$$\Phi(x,y)=\sum_{l=1}^{N_P}\varphi_l(x,y)\cdot c_l=\sum_{l=1}^{N_P}\left[\sum_{k=1}^{N_M}r_{kl}z_k(x,y)\right]c_l=\sum_{k=1}^{N_M}\left[\sum_{l=1}^{N_P}r_{kl}c_l\right]z_k(x,y) \tag{10}$$

The transfer function relating the mirror deflection expressed in the Zernike polynomial expansion as

$$\bar{\mathbf{\Phi}}=\tilde{\mathbf{R}}\cdot\bar{\mathbf{c}} \tag{11}$$

where $\bar{\mathbf{\Phi}}$ is the mirror surface response containing Zernike coefficients, $\tilde{\mathbf{R}}$ is denoted the control matrix defined by the elements r_{kl} where each column is an influence function of the mirror. The column contains the Zernike expansion coefficients representing the specific influence function.

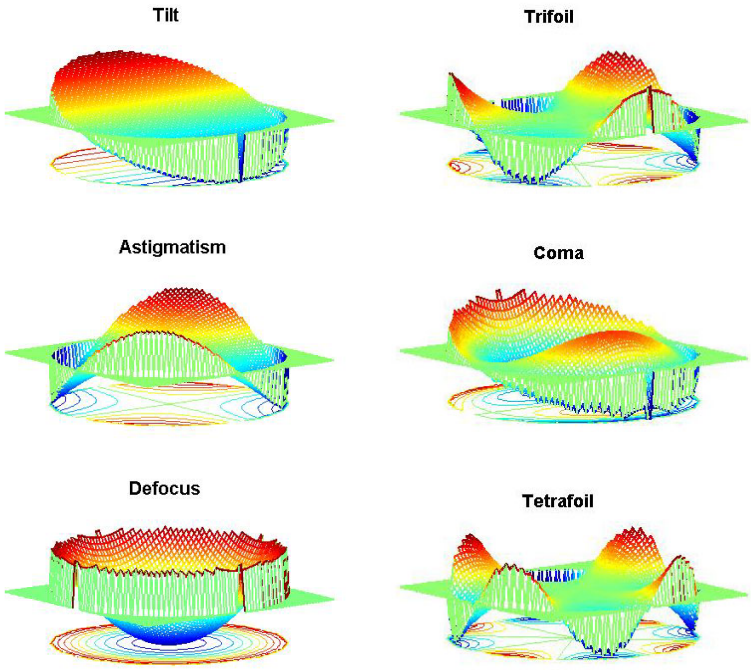

Figure 9 Example showing six normalised Zernike polynomials on a circular aperture. The polynomials were calculated using the labelling according to ref[12].

The influence function matrix, $\tilde{\mathbf{R}}$, has the dimension [N_MxN_P]. The vector, $\bar{\mathbf{c}}$, contains the control signals (voltages) applied to the mirror actuators. If the inverse of $\tilde{\mathbf{R}}$ is calculated the control signals required to generate a specified mirror surface can be determined as

$$\tilde{\mathbf{R}}^{-1} \cdot \bar{\mathbf{\Phi}} = \bar{\mathbf{c}} . \tag{12}$$

The inverse of the control matrix, $\tilde{\mathbf{R}}^{-1}$, can be determined using singular value decomposition (SVD). In the SVD scheme we express the influence matrix as

$$\tilde{\mathbf{R}} = \tilde{\mathbf{U}}\tilde{\mathbf{\Lambda}}\tilde{\mathbf{V}}^T \tag{13}$$

where $\tilde{\mathbf{U}}$ is an [N_MxN_M] orthogonal matrix, $\tilde{\mathbf{\Lambda}}$ is an [N_MxN_P] matrix diagonal and $\tilde{\mathbf{V}}^T$ is a [N_PxN_P] orthogonal matrix. The inverse can be calculated as

$$\tilde{\mathbf{R}}^{-1} = \tilde{\mathbf{V}}\tilde{\mathbf{\Lambda}}^{-1*}\tilde{\mathbf{U}}^T \tag{14}$$

where the $\tilde{\mathbf{\Lambda}}^{-1*}$ denotes the pseudo-inverse of $\tilde{\mathbf{\Lambda}}$. The SVD can be calculated using a standard mathematical package such as e.g. Matlab. The method outlined above was used to construct the transfer function expressed by eq. (11). The details describing the experimental procedure are presented in ref. [7].

2.2.4 Experimental results

The first experimental results were registered using only 19 channel of the DM mirror. The active actuators corresponded to the central ones. This mirror also had a maximum allowed voltage of 140 V. An example of observed interferograms using the 19 channel mirror and applying maximum voltage to all actuators is presented in Figure 10[6]. In this case no tilt term was added to the interferogram.

A) B)

Figure 10 A) Null interferogram corresponding to the DM mirror with no voltage applied to the actuators. B) Null interferogram with 140V applied to the 20 central actuators of the DM.

In Figure 10A the interferometer pattern without any voltage applied to the actuators is depicted. The part of the beam hitting the DM seems to be approximately planar since no stripes can be observed after adjustment of the interferometer. The interference pattern corresponding to 140V applied to 19 of the central actuators is shown in Figure 10B. A typical pattern of concentric circles attributed to spherical aberrations was observed. No major contribution from tilt or astigmatic terms was observed. After evaluation of the 19-channel mirror the second mirror having 37 available channels were studied in detail. Below some results from this study are presented[7].

The interferometer setup was extended by inclusion of Matlab written analysis code adapted for fringe analysis. The Fourier method described above was used residing on the work reported in the literature[13]. By introducing a tilt to the interferogram the Fourier components can be separated and the wavefront can be expressed in Zernike polynomials. The method is exemplified in Figure 11 where an interferogram consisting of a spherical aberration generated by the DM mirror is analysed. The interferogram is Fourier transformed (two-dimensional) and subsequently shifted and filtered (to remove the DC component and complex conjugate). By taking the inverse 2D FFT and unwrapping the phase the original phase distortion present in the wavefront can be extracted. The tilt is required to prevent overlap between the two spectral peaks since an overlap complicates the analysis considerably.

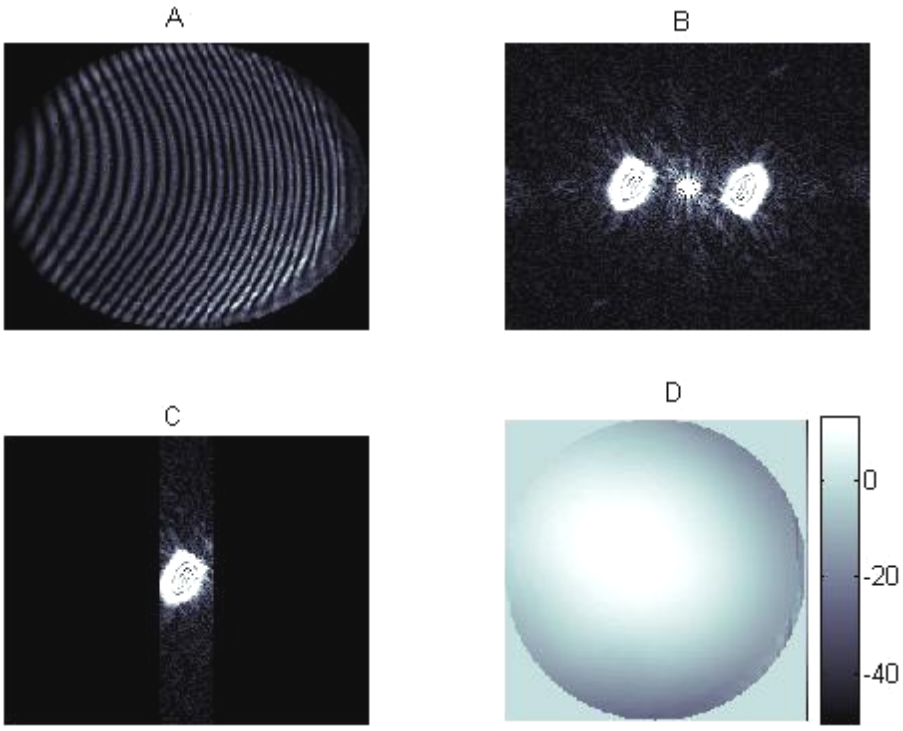

Figure 11 A) The interferogram captured by the CCD camera (consisting of a tilt and spherical aberration term) B) The Fourier transform of the interferogram depicted in A). C) Fourier transform after shifting and filtering. D) Reconstructed phase aberration after inverse Fourier transform and phase unwrapping. The scale is in radians.

The Fourier transform method was used to analyse the interferograms and determine the influence functions attributed to the DM mirror.

As mentioned above the mirror influence functions are required to construct the control matrix, $\tilde{\mathbf{R}}$. The influence functions can be determined by altering the voltage on a specific actuator keeping the rest at an optimised bias level. Following this procedure interferograms can be registered for each voltage setting and the Zernike decomposition determined. An example showing the influence function applying 200 V to actuator (no. 8) is shown in Figure 12.

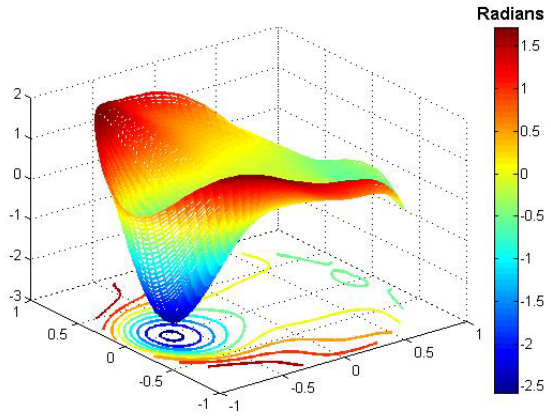

Figure 12 Example of the influence function of the mirror when 200 V is applied to actuator no. 8. The colorbar denotes the mirror membrane deviation in radians.

The mirror modes (eigenmodes) determine how well the DM mirror can reconstruct a given wavefront. The nine first modes corresponding to the studied 37 channel DM are presented in Figure 13. The modes were determined using the method briefly described above. These modes span the mirror sub-space and can be used to reconstruct a given aberration. The mirror modes correspond to diagonal values in the $\tilde{\mathbf{\Lambda}}^{-1*}$ matrix which are not equal to zero. The higher mirror modes have better capability to reconstruct higher spatial frequencies on the mirror surface.

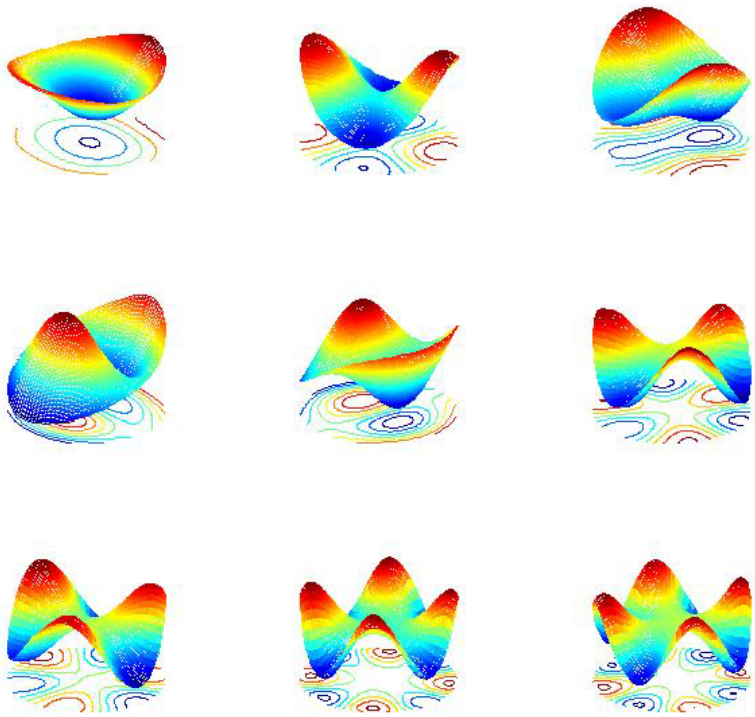

Figure 13 Experimentally determined mirror modes (eigenmodes) corresponding to the 37 channel DM mirror. Only the first nine eigenmodes are depicted.

The mirror is to be operated applying a voltage bias to the actuators. One issue to consider is to find the optimal bias to provide maximum dynamical range of the mirror. The features of the mirror were studied with different biases and one example showing a spherical bias is shown in Figure 14A. The corresponding Zernike coefficients verifies the dominating spherical term which corresponds to Zernike number three (Figure 14B).

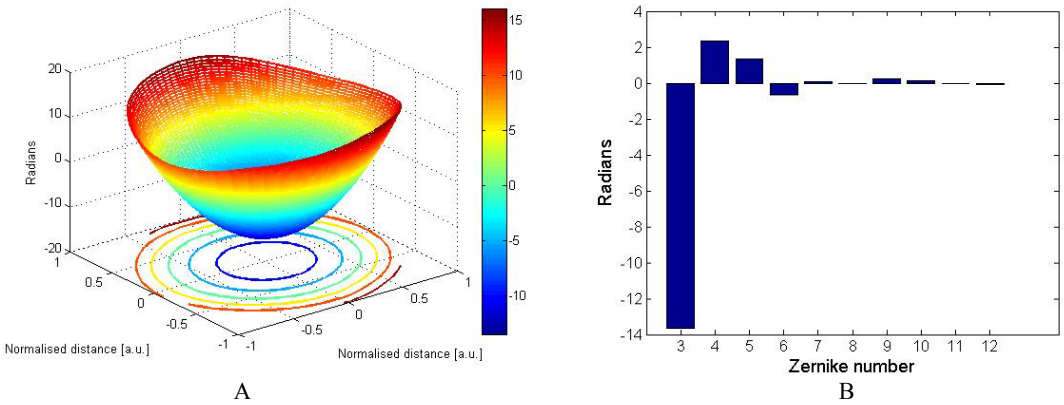

A B

Figure 14 A) Spherical bias applied to the DM mirror accomplished by applying 152 V to the actuators. B) Zernike coefficients corresponding to A).

The variation in the Zernike coefficients as a function of the bias applied to the mirror is illustrated in Figure 15 A and B. A bias about 152 V seems to provide the largest dynamical range of the Zernike coefficients. The spherical bias, on the other hand, provides a slightly larger range for the defocus term as expected.

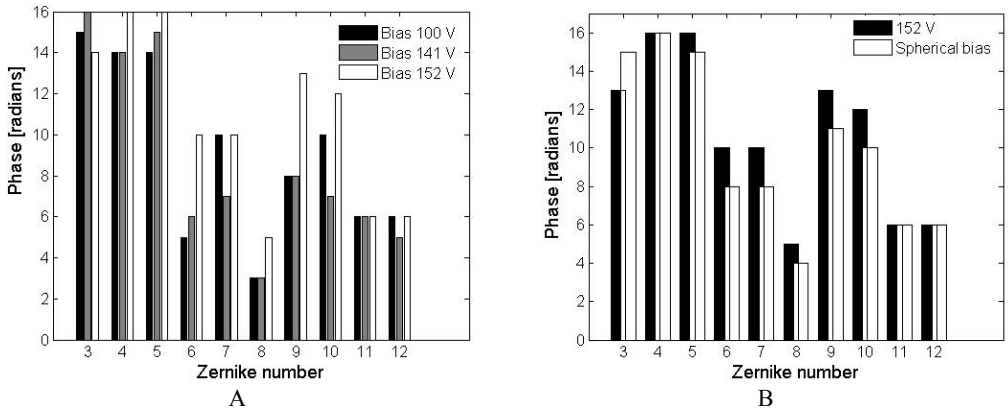

Figure 15 A) Variation of the Zernike polynomials as a function of the bias applied to the mirror. B) Same as A) but with spherical bias included.

The detailed analysis of the deformable mirror is presented in ref. [7]. The study gives information about the limitations and capabilities of the DM mirror with respect to generation of different Zernike polynomials. The study also provided detailed knowledge about the mirror performance and will facilitate the implementation into an adaptive optics system using a closed-loop reconstruction scheme.

2.3 Shack-Hartmann sensor

Several different methods exist to sense and reconstruct an aberrated wavefront. Among the most common method is the Shack-Hartmann (SH). The SH sensor was described in a previous report presenting some preliminary results and considerations. Below the SH principle is further considered and results from an experimental setup are discussed. In addition, the performance of some commercially available SH sensors are briefly compared.

2.3.1 Principle of the Shack-Hartmann wavefront sensor

The principle of the SH wavefront sensor is depicted in Figure 16A. As illustrated in the figure the lens array produces a spot pattern in the focal. An evenly spaced array of identical lenses will give an evenly spaced spot pattern on the CCD detector. If the wavefront is aberrated, on the other hand, the focus behind each lens shift laterally a distance proportional to the average wavefront tilt within the corresponding sub aperture (Figure 16B). From the distorted spot pattern the phase differences in the x and y directions can be calculated. The total phase distribution can subsequently be recovered from these phase differentials by using, for example, a least square fitting scheme.

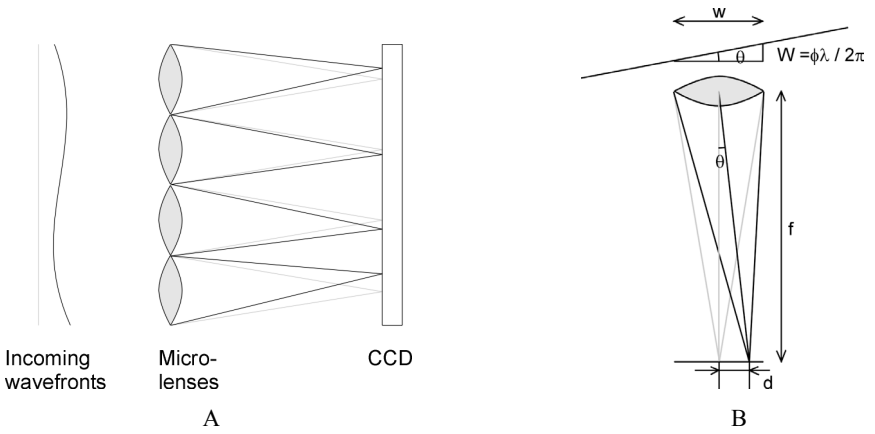

Figure 16 A) Principle of the Shack-Hartmann wavefront sensor. B) Geometrical relations for determining the local tilt of the wavefront.

A simple geometric relation between the tilt of the wavefront and the shift of the focus can be derived when the tilt angle is small and the lens is thin (Figure 16B). The incoming wavefront is tilted by an angle of θ (in front of the sub-aperture). It is assumed that the lens has a width w and focal length f, respectively.

The tilt introduces a phase delay, ϕ, between the two sides of the lens. The optical path difference (OPD) is the distance between the un-aberrated and the tilted wavefront. The difference in OPD from one side of the lens to the other is denoted W. If the phase delay ϕ is known the tangent of the tilt angle can be calculated according to

$$\tan\theta = \frac{\phi\lambda}{2\pi w}. \tag{15}$$

The shift of the focus is then given by

$$d = f\tan\theta = f\frac{\phi\lambda}{2\pi w}. \tag{16}$$

In a previous report the geometrical considerations above was utilised to calculate the expected deviations of the spot pattern for aberrations consisting of pure 2nd order astigmatism[6]. The simulation provided information about the order of magnitude the spot pattern was altered due to aberrations present in the wavefront.

2.3.2 Experimental results

A Shack-Hartmann sensor was tested using a commercially available Dalsa camera, CA-D1 progressive scan area camera and a micro lens array manufactured by Flexible OKO Optical. The Dalsa camera was interfaced to a National Instrument PCI-1424 digital image acquisition board for capturing images. A Labview interface was used to transfer images to the SH software. The Dalsa camera has a resolution of 128x128 pixels with 16 μm pixel size. The maximum frame rate is 736 frames/s. The micro lens array consisted of 16x16 orthogonal lenses having a focal length of 40 mm and a 0.3 mm centre distance between individual lenslets. The precision of the lenses were better than λ/8 waves.

The Shack-Hartmann sensor was explored using simple spherical aberrations. The static spherical phase aberration was incorporated by inserting a spherical lens with varying focal lengths in the beam path. Before each recording a reference image was required in order to

determine the centroid displacement which occurs due to the aberrations in the wavefront. An example showing a reference image and an aberrated spot pattern corresponding to a spherical aberration generated by the positive lens is depicted in Figure 17. The tilt term observed in the SH pattern was removed in the analysis. The translation of the individual spots can be observed induced by the spherical aberration.

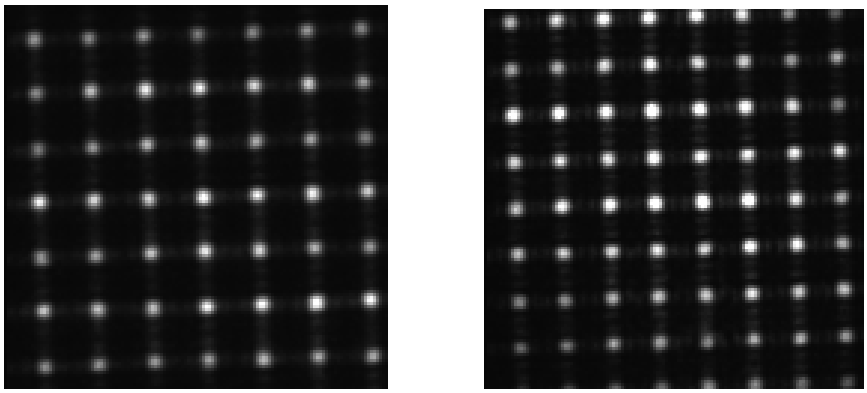

A B

Figure 17 A) Reference image captured by the SH sensor. B) Spot pattern corresponding to a static spherical aberration generated by a spherical lens having a focal length f = 300 mm.

In order to illustrate the effects originating from the individual lenslets the centre of gravity for each spot was calculated for the reference and aberrated wavefront (Figure 18). The translation of the individual SH spots due to the local tilt of the wavefront are evident. The motion of the spots is directed to the central part of the captured frame.

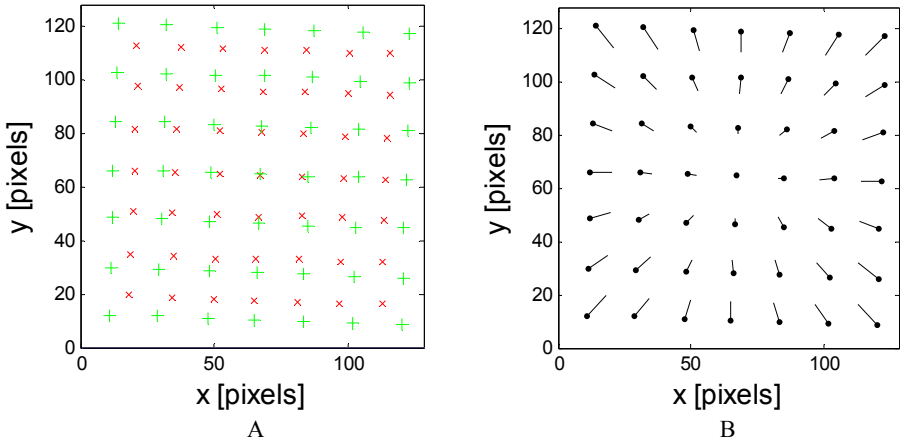

A B

Figure 18 A) Centre of gravity for the SH spots corresponding to the reference (+) and the aberrated (x) waves. B) Movements of the SH spots due to the spherical aberration. The focal length of the positive lens was f = 300 mm.

The theoretical calculations shown below (in paragraph “Simulations using LightPipes”) were also verified by experimental results. A 12x12 lens array was used in combination with a CCD camera. In Figure 19 is a reference image corresponding to a non-perturbed wavefront depicted. This spot pattern was utilised as a reference for calculation of sub-spot deviations due to wavefront aberrations.

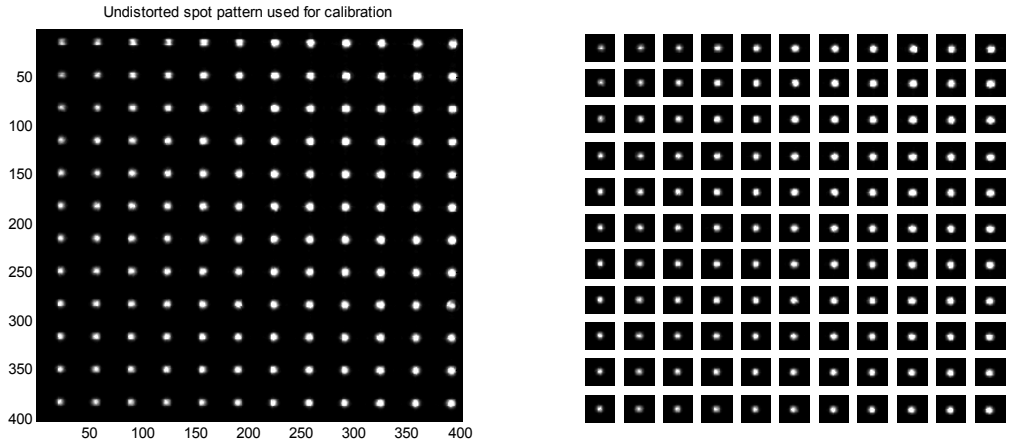

Figure 19 Image used for calibration (A) and calibration pattern divided into one image for each micro lens (B).

In order to introduce aberrations a spherical lens (with focal length of 750 mm) was used as a test object in this case. The spherical lens introduce a phase transformation which can be described as

$$t_l = e^{-\frac{k}{2f}(x^2+y^2)} \tag{17}$$

where f denotes the focal length, k the wave vector and x/y spatial coordinates. Hence, the lens gives rise to a spherical aberration.

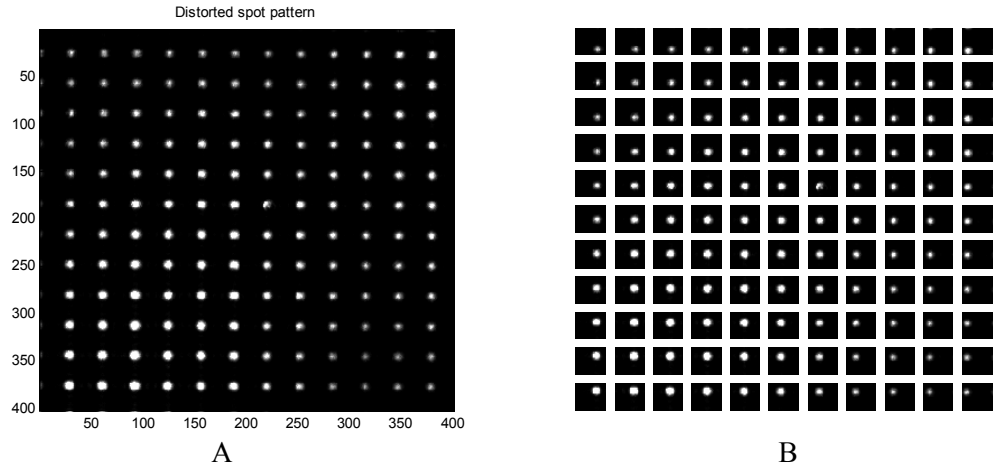

Figure 20 Spot pattern generated on the CCD when a 750 mm lens is inserted in front of the micro lens array (a) and distorted pattern divided into the regions defining the micro lens array (b).

Spot pattern observed when the 750 mm positive lens was used is shown in Figure 20. The phase distortion can be reconstructed from this pattern using the method described above. A reconstructed phase pattern is depicted in Figure 21A. The intensity pattern shows a spherical variation of the phase modulation. The theoretical phase variation attributed to a convex lens (having a focal length of 750 mm and applying eq. 17) is depicted in Figure 21B.

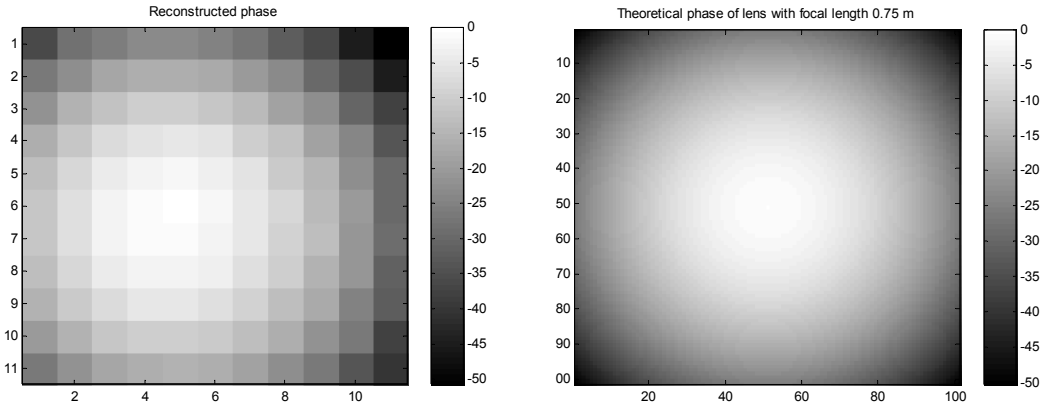

Figure 21 A) Reconstructed phase with least square fitting. B) Theoretical phase distortion of a 750 mm lens.

The spot pattern observed using the 750 mm convex lens but slightly tilted is shown in Figure 22A. In this case the translation of the individual spot due to the spherical aberration and the tilt can be observed.

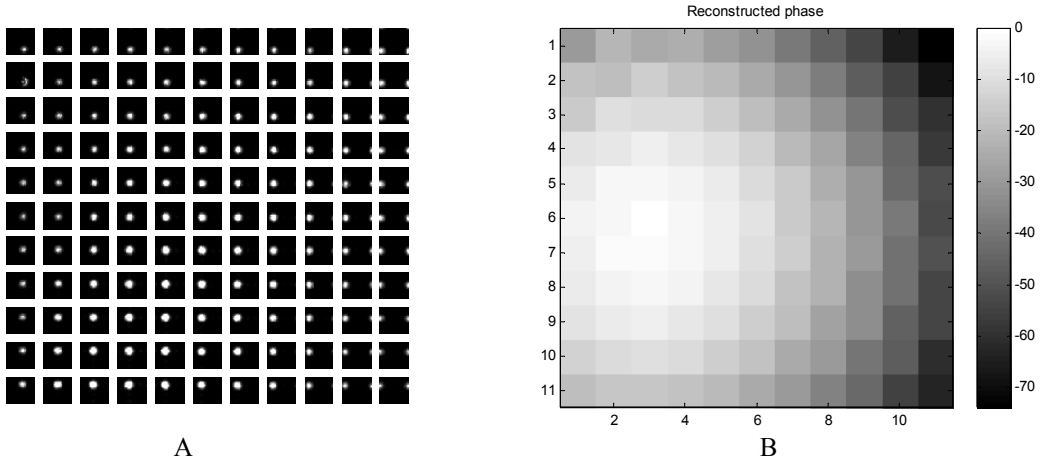

Figure 22 A) Spot pattern on CCD for the same 750 mm lens but horizontal tilted. B) Reconstructed phase for the horizontal tilted 750 mm lens.

The reconstructed phase corresponding to the aberrations (750 mm lens and the tilt contribution) is shown in Figure 22A. A slight movement of the centre of the spherical phase distortion can be observed in this case

2.3.3 Some commercially available Shack-Hartmann sensors

As a part of this work an inventory of commercially available Shack-Hartmann sensors was performed. The impetus for this investigation is due to the fact that acquiring a commercial SH sensor may probably be the most efficient way to obtain a reliable and robust sensor operating at moderate frame rates. Another issue of consideration is the software used for control or/and phase reconstruction. Commonly large efforts are required to implement the software. The motivation for developing "in house" dedicated software is the application driven requirements of very high closed loop bandwidth for the AO system. In this case specific computer accessories are required including e.g. FPGA or DSP techniques in combination with real-time programming software. However, running the WFS at lower bandwidth in initial studies seems necessary in order to fully understand limitations and schemes for performance optimisation.

Technical details (provided by the manufacturers) on some commercial Shack-Hartmann are summarized in *Appendix2 Some commercial Shack-Hartmann sensors*. The data is not claimed to represent all manufacturers, only the most renowned. Considering the performance of the studied SH sensors manufacturers which provide a sensor with accompanying control software (and also associated hardware) seems favourable. Closed loop architectures operating at bandwidth below 50 Hz seems to be available. However, if higher bandwidths are required a customer designed solution seems necessary.

3 MODELLING PERFORMANCE

Modelling components and sub-systems of the adaptive optical system is of considerable importance before the system is realised experimentally. The models can also be used to explain experimental results.

3.1 Shack-Hartmann sensor

A simple model based on geometrical optics was used to simulate the experimental Shack-Hartmann sensor setup. The SH sensor model was developed using the Optikwerk software running in windows on a PC[2]. The model allowed for variation of the optical layout of the SH sensor optimising the positioning and alteration of optical components. One issue to consider is whereas re-imaging lenses are required in order to optimise the usage of the available CCD detector area. An example showing the evaluated Shack-Hartman setup is depicted in Figure 23A. Here, a re-imaging lens was included to image the focal plane of the lenslet pattern onto the CCD detector. The distribution of the spots could be analysed by using spot analysis (Figure 23B).

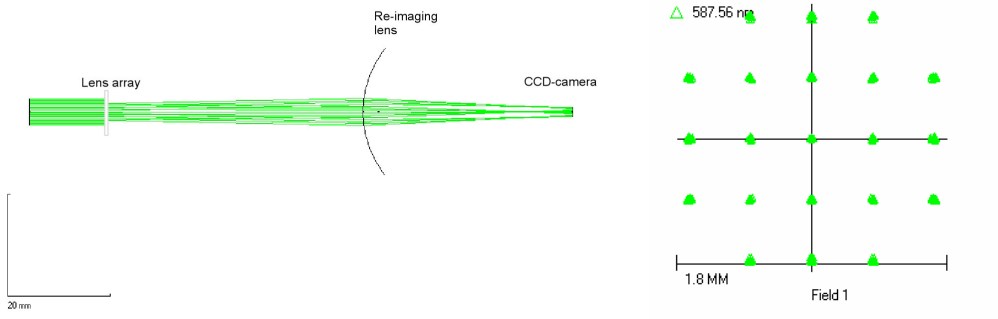

A B

Figure 23 A) Optical layout of the Shack-Hartmann sensor. B) Calculated spot diagram captured by the CCD camera assuming a plane wave impinging on the lenslet.

3.1.1 Simulations using LightPipes

The model described in this paragraph is an excerpt from a previous study where a simple model covering a Shack-Hartmann sensor was described[6].

[2] Optikwerk®, Optikwerk Inc., P.O. Box 92607, Rochester, NY 14692 USA

The geometrical simulations above give an idea of the result but do not include effects like diffraction and the size and form of each focus. In order to take these properties of the system into account simulations have been performed where a wave optics code, LightPipes, has been used to propagate the field to the CCD[14]. LightPipes does not support arrays of lenses but has a function for phase modulation of the optical field. To create an array of lenses the phase modulation attributed to one lens was replicated over the field.

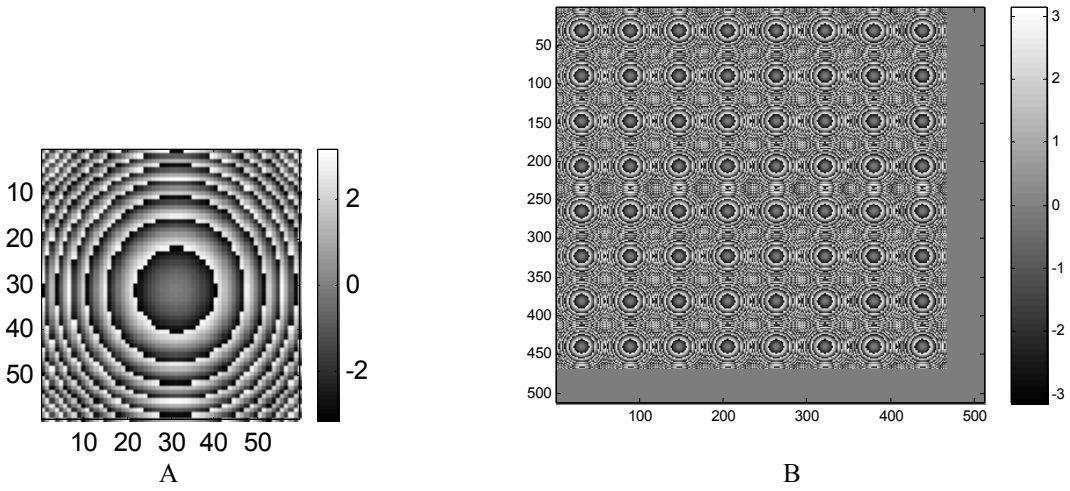

Figure 24 A) Phase modulation of one square aperture lens. B) Phase modulation of an array with square aperture micro lenses.

In Figure 24A the phase modulation from one square aperture lens is depicted. To obtain the corresponding phase modulation a plane wave has been propagated through a lens in LightPipes and then the phase distribution has been extracted. In Figure 24B the phase modulation have been replicated in both x and y direction to generate the effect of the lens array.

This phase distribution was subsequently added to the incoming aberrated phase and the resulting total field was propagated to the focal plane at the CCD. At the focal plane the field was interpolated to match the size and number of pixels on the CCD. The resulting spot pattern is shown in Figure 25. The intensity, size and form of the spots vary depending on the local phase features.

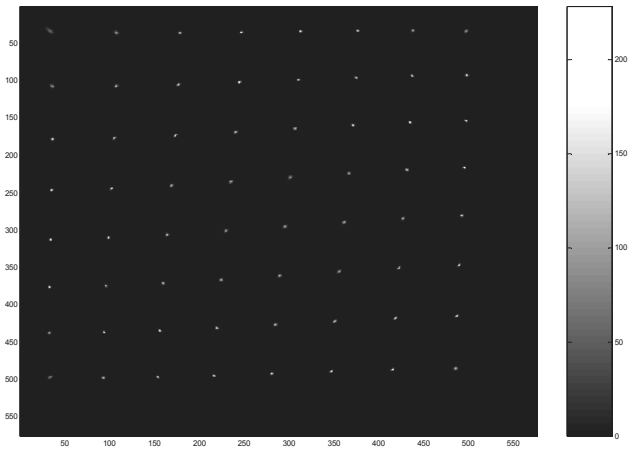

Figure 25 Spot pattern simulated with LightPipes.

In order to analyse the spot pattern simple image processing was performed on each aperture region. Setting a threshold and calculating the position of the centroid of the remaining blobs

determined the shift of focus. This method provides a rather straightforward way where the accuracy could be improved a lot. The geometrical equations were then used to transform these distances to phase differences. The phase differences in the x and y directions are shown in Figure 26A and B.

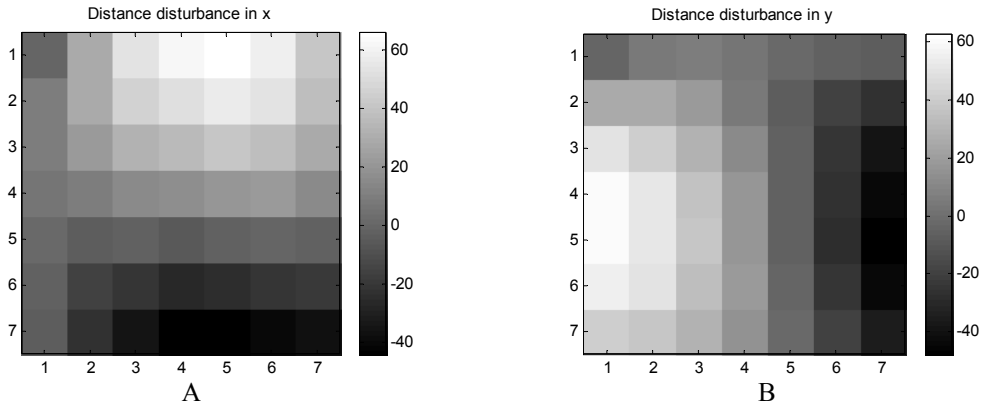

Figure 26 Shift of spots in x direction (A) and y direction (B).

The original phase was then reconstructed using a least square fit method[15]. The result is depicted in Figure 27A and B. The reconstructed phase agrees satisfactorily with the original phase (except for the lower resolution) It can also be observed that the Shack-Hartmann sensor only samples the wavefront with the frequency of the lens array, i.e. an 8x8 array gives 8x8 phase values.

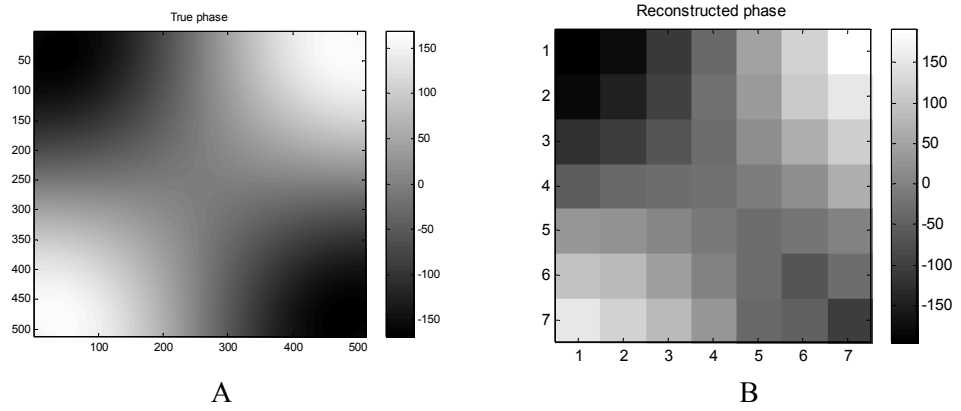

Figure 27 A) Original phase corresponding to astigmatism, see ref[6]. B) Least square fit estimated phase distribution.

3.2 Deformable mirror

An effort to model the deformable mirror has been initiated. The idea is to use the finite element method provided by FEMLAB[3] to model the deflection of the mirror membrane caused by the electro-statically forces induced when a voltage is applied to the actuators. The calculated deflection of the membrane can be interpreted in wavelengths or phase modulation by considering the optical path difference from a given reference position of the membrane.

[3] FEMLAB 3.1, Comsol AB, see http://www.euro.comsol.com/

The electro-statically forces controlling the membrane structure is governed by the Laplace equation with appropriate boundary conditions (BC). The Laplace equation assuming small mirror deflections can be written according to[16]

$$\nabla^2 S(x,y) = -\varepsilon_0 \frac{\left[V(x,y)\right]^2}{Td^2} \tag{18}$$

where *S(x,y)* is the shape of deflection of the membrane, *V(x,y)* is the applied voltage, *T* is the membrane tension, ε_0 is permittivity of vacuum and *d* is the distance between the actuator structure and the mirror. Equation (18) can also be expressed in terms of the pressure *P(x,y)* distribution

$$\nabla^2 S(x,y) = -\frac{P(x,y)}{T}. \tag{19}$$

By solving the Laplace equation using appropriate BC the deflection of the membrane for different voltage distributions applied to the actuators can be calculated.

In a FEMLAB model the two-dimensional (2D) model comprising the mirror membrane and the geometry of the underlying actuator structure can be defined. The actuator structure is a 2D mesh defining the hexagonal actuator structure. The structure is confined by a circular aperture defining the size of the overlying membrane. The advantage of using FEMLAB is the powerful interface, capability of solving multi-physics problems, the visualisation properties and the connectivity to Matlab. Currently the model is under definition and to be evaluated in near future. The calculated mirror deformations can (after calibration of the model) be utilised to compare calculated mirror performance with experimental results.

4 LABORATORY CLOSED LOOP ADAPTIVE OPTICS SYSTEM

In this paragraph an experimental setup for a closed-loop AO system based on the components discussed above is suggested. The motivation for the system is to explore issues related to understanding and development of closed-loop control schemes and algorithms. The system should include a SH wavefront sensor (developed in house or commercial), a tip-tilt mirror, a quadrant detector and a deformable mirror. The aim is to develop a system operating at approximately 25 Hz closed-loop bandwidth. Hardware dedicated for control and reconstruction should be identified. One possibility which has been considered is to run the system in a real-time application associated with LabView on a PXI computer as a standalone application. The advantage of using this environment is the flexibility provided during development.

A schematic experimental setup for closed loop AO test bed to be implemented on an optical table is outlined in Figure 28. A spatial light modulator is incorporated to generate dynamical aberrations. The system includes both tip-tilt and high order corrections. If the tip-tilt error can be registered using the SH sensor the quadrant detector can be neglected and the possibility to increase the bandwidth.

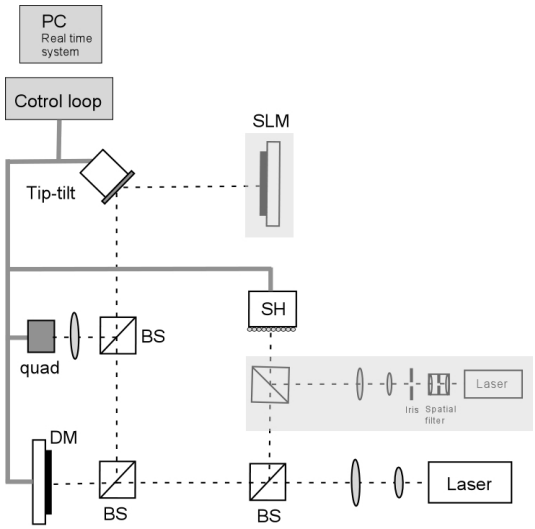

Figure 28 Schematic layout of a closed-loop adaptive optics setup on an optical table. The following abbreviations are used: BS = Beam splitter, DM = deformable mirror, SH = Shack-Hartmann sensor, SLM = Spatial light modulator, quad = quadrant detector. The laser indicated in gray may be included to provide a reference signal for the SH sensor if not absolutely calibrated.

One way to generate dynamical phase aberrations is to use a spatial light modulator based on liquid crystals[17]. In order to illustrate how these components can be employed in a laboratory setup for generation of known wavefront aberration a simple example is presented below. The principle was tested using a Shack-Hartmann sensor and applying different phase distributions to a 128x128 nematic liquid crystal spatial light modulator (SLM). The images were captured by a CCD camera. The diffraction effects in the pixel structure of the SLM results in small patterns at each focus instead of smaller spots.

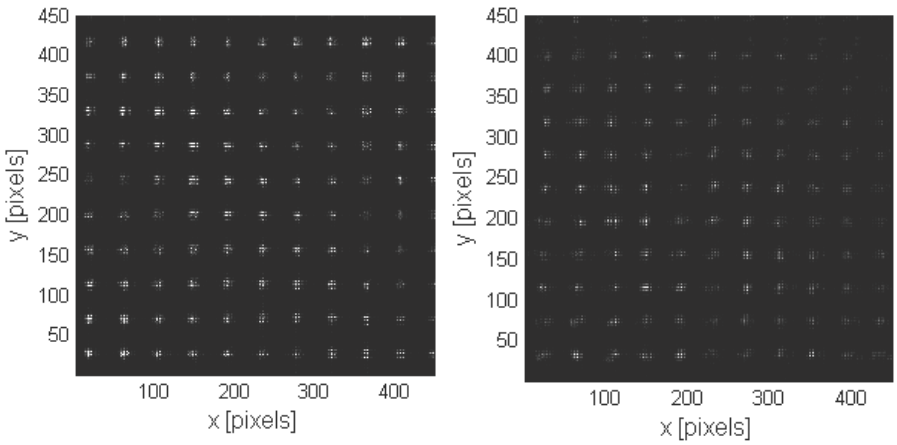

Figure 29 Shack-Hartmann image of the 128x128 NLC SLM in off position (left) and with a quadratic phase modulation (right) implemented.

The centroid position of each focus was determined and the movement of each spot after applying a quadratic phase distribution is presented in Figure 30. The motion of the spots verifies that the aberration corresponds to a quadratic phase transformation.

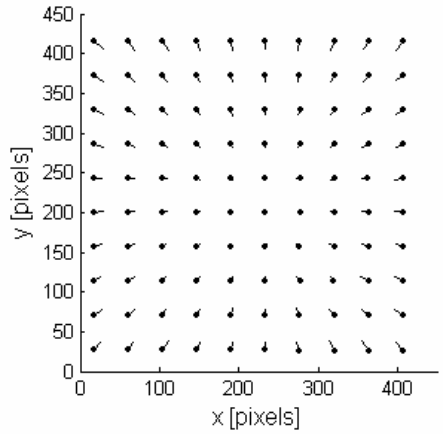

Figure 30 Movements of spots indicated by short lines when applying a quadratic phase distribution to the SLM. The dots indicate centroid positions in reference image. The tilt aberration was removed before the analysis.

The advantage of using a SLM for aberration generation is the possibility to generate known aberration patterns at different frame rates (limited by the update frequency of the SLM). Well characterised SLMs, with respect to phase and amplitude modulation of planar wavefronts, are available. Alternatively, static phase aberrations can be introduced into the system.

5 DISCUSSION AND CONCLUSIONS

In this report we have reviewed some activities related to adaptive optics. Different parts constituting an adaptive optics system have been considered. The components discussed include the WFS focussing on the Shack-Hartmann principle, the correction element being a membrane deformable mirror and a tip-tilt corrector. Reconstruction schemes and modelling have also briefly been considered. The main technical work was related to detailed characterisation of the deformable mirror and is to be reported in a separate work[7].

The Shack-Hartmann scheme for WFS has been studied both experimentally and by modelling efforts. A physical optics model was developed constituting of a microlens array and the CCD detector. From the deflection of the SH spot pattern wavefront aberrations could be reconstructed. In addition, an experimental SH setup was modelled by a ray-tracing code to optimise the design. Experimental studies were subsequently carried out considering simple spherical aberrations and the effects in the SH pattern. The wavefront could be reconstructed but the scheme was limited by the software. It is concluded that acquiring a commercial SH sensor for future closed loop studies needs to be considered. Applications requiring very high bandwidth, such as turbulence compensation, suggest that studies of implementing fast SH schemes should be performed.

A 37 channel deformable membrane mirror has been characterised in detail. A method based on Fourier analysis of interferometric data was used to analyse the modal characteristics of the mirror. The properties of the mirror while altering control signals were studied in a Twyman-Green interferometer setup. Software was developed capable of decomposing the mirror responses in Zernike polynomials and determining the mirror eigenmodes. The mirror transfer function, describing how the mirror alters for different control signals was determined. Moreover, residual aberration, optimal bias setting and performance limitations are example of other issues that were considered. The spatial properties of the mirror is now well characterised for future implementation into a closed-loop AO system.

As pointed out above the long term purpose of this work is to develop a closed-loop adaptive optics system implemented in a laboratory setup. The AO-system may incorporate the component discussed in this report i.e. the SH WFS, a tip-tilt mirror and a membrane

deformable mirror. The system should aim to be capable to correct low order aberrations. On way to inject known aberrations into the system is to use a spatial light modulator. The SLM allows dynamical update of the aberrations at rates in the same range as the imagined AO-system. The ambition is to close the loop and aim for a closed-loop temporal bandwidth of about 25 Hz. The motivation for the system is to gain knowledge about performance and limiting factors for subsequent emphasis on temporal bandwidths relevant for correction of atmospheric turbulence i.e. of the order of 500 Hz.

6 APPENDIX 1 TECHNICAL SPECIFICATIONS OF THE TIP-TILT MIRROR

The investigated tip-tilt mirror (S-334.2SL) was a two-axis piezoelectric mirror fabricated by Physike Instrument GMbH. The angular resolution of the mirror is 0.5 µrad and the maximum angular deflection approximately 50 mrad. The resonance bandwidth of the piezoelectric tip-tilt mirror is specified to be 1 kHz. All technical data for the tip-tilt mirror is presented in Table 1.

Table 1 Technical data for the tip-tilt mirror

Technical Data

Models	S-334.2SL
Active Axes	θ_X, θ_Y
*Open-loop tilt angle @ 0 to 100 V	50 mrad (±25 mrad) ±20%
*Closed-loop tilt angle	50 mrad (±25 mrad)
Integrated feedback sensor	full-bridge strain gauge sensors
Closed-loop / open-loop angular resolution	< 5 / 0.5 µrad
Closed-loop linearity (typ.)	±0.25%
Electrical capacitance	3.6 µF/axis ±20%
Resonant frequency with 10 mm diam. x 2 mm glass mirror	1.0 kHz ±20%
Resonant frequency with 12.5 mm diam. x 2.5 mm glass mirror	0.8 kHz ±20%
Distance of pivot point to platform surface (lower mirror surface)	2 ±0.5 mm
Operating temperature range	-20 to 80 °C
Voltage connection	3 x LEMO FFA.00.250 male, 2 m
Sensor connection	2 x LEMO FFA.0S.304 female, 2 m
Weight (without cables)	65 g ±5%
Standard mirror	diameter: 10 mm, thickness: 2 mm, BK7, λ/5, R > 98% (λ = 500 nm to 2 µm)
Material casing	Titanium

** Mechanical tilt, optical beam deflection is 100 mrad.*

(from Physike Instrument, see URL[4])

[4] http://www.physikinstrumente.de/

7 APPENDIX2 SOME COMMERCIAL SHACK-HARTMANN SENSORS

In this appendix the performance some relevant commercial Shack-Hartmann sensors are summarised.

Haso, Imagine Optics (http://www.imagine-optic.com)
Imagine Optics manufactures three different SH sensors as indicated in Table 2. The performance of the sensor varies whereas the sensor with highest resolution (HASO64) operates at lower acquisition frequency. Imagine Optics provide complete solutions for AO setups by incorporating different deformable mirrors (see below). The highest closed loop bandwidth is obtained with HASO16 operated in a DOS environment.

Table 2 Technical data – HASO Shack-Hartmann sensor (Imagine Optics, data extracted from web)

	HASO 16	HASO 32	HASO 64
Aperture dimension	2,5 x 2,5 mm^2	5 x 5 mm^2	12 x 12 mm^2
Number of sub-apertures dedicated for analysis (1)	16 x 16	32 x 32	64 x 64
Tilt dynamic range	> ± 3 ° (260 λ)	> ± 3 ° (520 λ)	> ± 3 ° (1200 λ)
Focus dynamic range	± 0,025 m to ± ∞ (50 λ)	± 0,025 m to ± ∞ (200 λ)	± 0,04 m to ± ∞ (800 λ)
Repetability (rms)	< λ/200		
Wavefront measurement accuracy in absolute mode rms (2)	λ/100		
Wavefront measurement accuracy in relative mode rms (3)	λ/150		
Tilt measurement sensitivity	6 µrad	3 µrad	1 µrad
Focus measurement sensitivity	5.10^{-3} m^{-1}	10^{-3} m^{-1}	5.10^{-4} m^{-1}
Spatial resolution	~160 µm	~ 160 µm	~ 190 µm
Max acquisition frequency	955 Hz	77 Hz	20 Hz (opt. 40 Hz)
Processing frequency	8-40 Hz	4-20 Hz	2-10 Hz
Working wavelength	350-1100 nm		
Calibrated wavelength band	400 - 600 nm / 500 - 700 nm / 650 - 900 nm / 800 - 1100 nm		
Extended calibrated wavelength band	400 - 700 nm / 500 – 900 nm / 650 - 1100 nm		
Working temperature	15 - 30 °C		
Dimensions / weight	90x100x130 mm / 1125 g	80x90x100 mm / 980 g	90x100x130 mm / 1200 g
Power supply	5,-12,12 V / 6 W	5,-12,12 V / 6 W	+5,-5,-15,28 V / 20 W

Manufacturer	Mirrors			Drivers Windows
	Nom	Actuateurs	Diamètre utile	
CILAS	BIM 31	31	55 mm	Available
	BIM 36	36	62 mm	Available
	BIM 60	60	60 mm	Available
	SAM 48			Available
IPLIT		19	40 mm	Available
XINETICS		37	50 mm	Available
OKO	DM 37	37	15mm	Available
HAMAMATSU	X8077	480*480	25mm	Available

HASO Version	Standard configuration (Windows interface)	Fast Close loop (DOS interface)
HASO 64	2 Hz *	20 - 40 Hz *
HASO 32	7 Hz *	77 Hz *
HASO 16	10 Hz *	900 Hz *

WaveScope, Adaptive Optics Inc. – AOI (http://www.aoainc.com)
Adaptive Optics Inc. has long experience in manufacturing of WFS in adaptive optics applications. The Shack-Hartmann sensor is labelled WaveScope and exists in different configurations as indicated in Table 3.

Table 3 WaveScope manufactured by AOI

Model Number	Wavelength Range [nm]	Lens Pitch [µm]	Lens Array Format	Frame Rate [Hz]	Camera Bits	External Trigger	Exposure Control	Application
WFS-01	400 - 1064	480 300 190	20 x 20 32 x 32 72 x 72	30	8	no	yes	Optical component measurement. CW laser wavefront and beam profile. Low bandwidth adaptive optics.
WFS-UV	193 - 400	300	32 x 32	30	8	no	yes	Optical component measurement. Excimer laser wavefront and beam profile.
WFS-mini	400 - 1064	250 190	20 x 20 26 x 26	30	8	no	yes	Low cost wavefront phase measurements. IR and UV versions available.
WFS-IR1	900 - 1700	480 300 190	20 x 20 32 x 32 72 x 72	30	8 or 12	yes	yes	Pulsed laser wavefront and beam profile of Nd:YAG and soild state communications lasers
WFS-IR2	2000 - 20,000	call	call	30	8 or 10	yes	yes	Mid IR laser wavefront and beam profile. Wavefornt phase of CO_2 lasers.
WFS-F1	400 - 1064	call	call	490	12	yes	yes	Pulsed visible laser wavefront, Ti:sapphire. Medium bandwidth adaptive optics.
WFS-F3	400 - 1064	call	call	700	8	yes	yes	Astronomical adaptive optics and laser communications.
AO	With a WaveScope sensor makes a complete adaptive optics system. Includes an optical bench, far field imaging camera, monitors, collimated HeNe laser, reference mirror, beamsplitters, and a 37 actuator micro-machined deformable mirror with drive electronics, power supplies, and control software.							Closed loop adaptive optics. Laser wavefront control.
DM	37 actuator micro-machined deformable mirror with drive electronics, power supplies, and contol software.							Closed loop adaptive optics. Laser wavefront control.
DM-XIN-xxx	PC Interface electronics and control software for Xinetics xxx actuator mirror							Mirror flattening and control

Technical data – WFS-01

Aperture	5 mm diameter
Frame rate	30 Hz
Pupil shape	circular, rectangular, obscured
Wavelength range	400 to 1064 nm
Wavefront sampling	20 x 20, 26 x 26
Gradient accuracy	λ/20 P to V @ 633 nm
Tilt dynamic range	80λ P to V @ 633 nm
RMS wavefront error	λ/100 @ 633 nm

Exposure control	1/60 to 1/10,000 second
Data collection	30 Hz burst, wavefront averaging
Output	ASCII, binary, FITS, TIF, GIF, BMP, PS, JPG, Code V and Zemax compatible Zernikes. Wire, contour and text displays.
Measurements	Spot images, gradient vectors, OPD, PSF, MTF, encircled energy, fringes, beam profile, laser beam quality, Zernike, monomial, Seidel, Hermite, Chebychev and Legendre polynomials.

Technical data – WFS-mini

Aperture	10 mm diameter
Frame rate	30 Hz
Pupil shape	circular, rectangular, obscured
Wavelength range	400 to 1064 nm
Wavefront sampling	20 x 20, 32 x 32, 72 x 72
Gradient accuracy	λ/20 P to V @ 633 nm
Full aperture tilt range	400λ P to V @ 633 nm
RMS wavefront error	λ/100 @ 633 nm

Exposure control	1/60 to 1/10,000 second
Data collection	30 Hz burst, wavefront averaging
Output	ASCII, binary, FITS, TIF, GIF, BMP, PS, JPG, Code V and Zemax compatible Zernikes. Wire, contour and text displays.
Measurements	Spot images, gradient vectors, OPD, PSF, MTF, encircled energy, fringes, beam profile, laser beam quality, Zernike, monomial, Seidel, Hermite, Chebychev and Legendre polynomials.

Technical data – WFS-IR

Aperture	10 mm diameter
Frame rate	30 Hz
Pupil shape	circular, rectangular, obscured
Wavelength range	0.9 to 1.7 µm
Wavefront sampling	20 x 20, 32 x 32, 72 x 72
Gradient accuracy	λ/20 P to V @ 633 nm
Full aperture tilt range	400λ P to V @ 633 nm
RMS wavefront error	λ/100 @ 633 nm

Exposure control	1/60 to 1/10,000 second
Data collection	30Hz burst, wavefront averaging
Output	ASCII, binary, FITS, TIF, GIF, BMP, PS, JPG, Code V and Zemax compatible Zernikes. Wire, contour and text displays.
Measurements	Spot images, gradient vectors, OPD, PSF, MTF, encircled energy, fringes, beam profile, M-squared, Zernike, monomial, Seidel, Hermite, Chebychev and Legendre polynomials.

As noted in the data above WaveScope is also available with control software and correction element to constitute a full closed loop adaptive optic system operating at lower bandwidth.

FrontSurfer, OKO Technologies (http://www.okotech.com)
The FrontSurfer WFS is not a true Shack-Hartmann sensor since a Hartmann mask is used instead of the lens array. One drawback of using a Hartmann mask in favour to a lens array is the lower fill factor since the lens array does averaging over each individual lenslet.

Table 4 Data extracted from the FrontSurfer manual (ver. 1.3, 2003)

Sensitivity	**Wavelength**	**Acquisition rate**	**Calibration**	**No apertures**
< λ/40 rms	VIS-NIR	< 1 KHz	Absolute/reference	30x40 sub apertures
Aperture	**Closed loop**			
3.5 mm	12.5 Hz			

Other manufacturer also present technical data but the emphasis on their products is on applications which not require high bandwidths.

8 REFERENCES

[1] L. Sjöqvist and O. Steinvall (Eds.), "CEPA8 JP8.11Laser Beam Steering – System Study", FOI Report, *FOI-R--01235--SE*, 2004.

[2] L. Sjöqvist, "Adaptive optics in laser countermeasure applications", *FOA report*, *FOA-R--00-1736-612--SE,* 2001.

[3] J. M. Geary, "Introduction to wavefront sensors", *SPIE Press*, vol. TT 18, Bellingham, 1995.

[4] R.B. Schack, B. C. Platt, *JOSA A*, vol. 61, p. 656, 1971

[5] R. K. Tyson (ed.), "Adaptive Optics Handbook", Marcel Dekker Inc., Basel, 2000.

[6] L.Sjöqvist, E. Hällstig, "Studies of a Schack-Hartmann wavefront sensor and a membrane deformable mirror–some preliminary results", *FOI MEMO 03-2994*, 2003.

[7] U. Larsson, "Experimental characterisation of a membrane deformable mirror", To be published, *FOI Report*, 2004.

[8] QuickFringe 4, Reference manual, Diffraction Limited Inc.

[9] L. Zhu, P-C. Sun, D-U. Bartsch, W. R. Freeman and Y. Fainman, "Wave-front generation of Zernike polynomial modes with a micromachined membrane deformable mirror", *Appl. Optics*, vol. 38, pp. 6019-6026, 1999.

[10] L. Zhu, P-C. Sun, D-U. Bartsch, W. R. Freeman and Y. Fainman, "Adaptive control of a micromachined continuous-membrane deformable mirror for aberration control", *Appl. Optics*, vol. 38, pp. 6019-6026, 1999.

[11] E. J. Fernandez and P. Artal, "Membrane deformable mirror for adaptive optics: performance limits in visual optics", *Optics Express*, vol. 11, pp. 1056-1060, 2003.

[12] D. Malacara, "Optical Shop Testing", 2nd Ed, John-Wiley, NewYork, 1992.

[13] M. Takeda, H. Ina and S. Kobayashi, "Fourier transform method of fringe pattern analysis for computer based topography and interferometry", *J. Am. Opt. Soc.,* vol. 72, pp. 156-160, 1981.

[14] G.Vdovin and F. van Goor, "LightPipes Optical Toolbox", OKO Technologies, 2002

[15] David L Fried, "Least-square fitting a wave-front distortion estimate to an array of phase-difference measurements", *J. Opt. Soc. Am.* Vol. 67 No. 3, p 370-375, March 1977

[16] E. Scott and N. Baraket, "Configuring an electrostatic membrane mirror by least-square fitting with analytically derived influnce functions", *JOSA A*, vol. 3, pp. 1833-1839, 1986.

[17] E. Hällstig and references therein, "Nematic liquid crystal light modulators for laser beam steering", *Comprehensive summaries of Uppsala Dissertations from the Faculty of Science and Technology*, no. 1048, Uppsala university, ISBN 91-554-6110-7, 2004.